Correction: 19 March 2008

www.sciencemag.org/cgi/content/full/1155400/DC1

Supporting Online Material for

Coherent Dynamics of a Single Spin Interacting with an Adjustable Spin Bath

R. Hanson,* V. V. Dobrovitski, A. E. Feiguin, O. Gywat, D. D. Awschalom

*To whom correspondence should be addressed. E-mail: r.hanson@tudelft.nl

Published 13 March 2008 on *Science* Express
DOI: 10.1126/science.1155400

This PDF file includes:

Correction (19 March 2008): An older, incorrect version of the SOM was originally posted. The correct SOM file is now available.

1 Experimental Methods

1.1 Measurement setup

The NV center spins are imaged, initialized and read out using a confocal microscope at room temperature. The magnetic field is aligned along the [111] axis of the diamond sample. The NV centers studied in this work are formed during growth in a type Ib single-crystal diamond from Sumitomo Electric. This diamond contains nitrogen (N) impurities with a density of $10^{19} - 10^{20}$ cm^{-3}. The dipolar interaction strength between electron spins is therefore of order MHz.

Single NV centers are identified by observing antibunching in photon correlation measurements (demonstrating that it is a single emitter) and measurement of the spin splitting at zero magnetic field (showing it is an NV center). The NV centers studied here were selected to have their symmetry axes parallel to the magnetic field, so that mixing of electronic spin levels is minimized. Details about the optics part of the setup, the identification of single NV centers and about the magnetic field alignment can be found in Ref. S1.

We use magnetic resonance to coherently manipulate the electron spin state. An oscillating radiofrequency (RF) current is sent through a thin gold wire (10 micrometer diameter) which generates an oscillating RF magnetic field. The wire is positioned to within about 20 micrometer of the NV center under study. Multiple synchronized outputs of a pattern generator (HP 81130A) are used to control the laser via an acoustic-optical modulator (Isomet 1250C), to gate the photon counters, and to trigger an arbitrary wave-form generator (Tektronix AWG520). The arbitrary waveform generator in turn chops a continuous-wave RF signal (Agilent E8257C) through an RF switch (Minicircuits ZA-SWA-2-50DR), leading to the desired sequence of RF bursts. Risetime of the RF pulses after the switch is about 1 nanosecond. In order to obtain high driving powers the RF signal is amplified with up to 40 dB (Amplifier Research 25S1G4A).

1.2 Spin manipulation sequences

The pulse duration needed to achieve a 90-degree rotation (π/2 pulse) or a 180-degree rotation (π pulse) of the spin is calibrated from coherently driven spin oscillations. The π pulse is defined as a pulse which inverts the z-projection of the spin, i.e. transforms S_0^z operator of the NV center electron spin to $-S_0^z$. The $\pi/2$ pulse is twice shorter. All pulse sequences start by initializing into $|m_S = 0\rangle$. At B = 0 G, all three spin sublevels are manipulated. A π/2 pulse creates the spin superposition state $1/\sqrt{2}\,(|m_S = -1\rangle + |m_S = +1\rangle)$ (up to a global phase). In the Ramsey experiments, dephasing of this state is measured by applying a second π/2 pulse after a variable free evolution time. In case no phase difference is acquired, this second pulse brings the system back to the initial state $|m_S = 0\rangle$. At B = 740 G, we only manipulate the spin sublevels $|m_S = 0\rangle$ and $|m_S = -1\rangle$ (the state $|m_S = +1\rangle$ is far away in energy and does not contribute to the dynamics). Since at high fields we are dealing with only two levels, the calibration of $\pi/2$ and π pulses is different from the zero-field case where we manipulate all

three spin sublevels. In particular, a $\pi/2$ pulse on this effective two-level system (effective spin 1/2) creates the spin superposition state $1/\sqrt{2}\,(|m_S=-1\rangle + |m_S=0\rangle)$ (up to a global phase). In the Ramsey experiments, the second $\pi/2$ pulse now creates the state $|m_S=-1\rangle$ in case of no dephasing. As a consequence, the Ramsey curves at B = 0 G and at B = 740 G have opposite initial values in our experiments (see Fig. 2A).

To measure the coherence time T_2 a π pulse is inserted in between the two $\pi/2$ pulses, see Fig. S1A. Fig. S1B shows measurements on NV31 at B= 0 G where the free evolution time before the π pulse, τ_1, is fixed, and the free evolution time after the π pulse, τ_2, is varied. A clear echo signal is obtained whenever τ_1 = τ_2, demonstrating that part of the dephasing can be reversed. Note that both at B = 0 G and at B= 740 G, the echo sequence ideally brings the system back to the initial state $|m_S=0\rangle$ (up to a phase factor), since the total rotation is over an angle of 2π. As expected, the observed oscillations as a function of τ_2 are similar to those obtained from the Ramsey experiments (see Fig. 2A). By setting τ_1 = τ_2 =τ and varying the total free evolution time 2τ , a spin echo measurement is performed (see Fig. S1C).

2 Theoretical description of the system

We consider decoherence of a single NV center in diamond by a bath of the electron spins of the nitrogen atoms (P1 centers, according to classification of Ref. S2). The NV center is treated as a localized spin $S_0 = 1$, possessing a single-axis anisotropy $H_a^0 = D(S_0^z)^2$, where $D = 2.87$ GHz is the splitting between the levels $|m_S=0\rangle$ and $|m_S=\pm1\rangle$ (here m_S denotes the eigenstates of S_0^z) at zero external magnetic field. The anisotropy z-axis is directed along the $[111]$ direction. The quantity measured in experiments is $p_0(t)$: the time-dependent population probability of the state $|m_S=0\rangle$. The initial state of the NV center is $|m_S=0\rangle$, while the state of the bath is maximally mixed: the density matrix of the bath is proportional to the identity matrix, i.e. all states of the bath are equally probable.

The nitrogen P1 centers are treated as localized spins $S_k = 1/2$ ($k = 1, \ldots N$). For given experimental circumstances (large average distance between the NV center and the nitrogens), the dominant coupling between the NV center and the nitrogens (the system-bath interaction H_{SB}) is due to the dipolar interaction. Also, the dipolar interaction between different bath spins is important, since the typical distance between different nitrogens is the same as the typical distance between NV and a nitrogen. Finally, we must take into account the hyperfine interactions on the NV site and on the P1 sites, since the electron spins at both NV and P1 sites interact with the nuclear spin of ^{14}N.

Decoherence of a central spin by a spin bath is a very complex many-body non-equilibrium quantum phenomenon, which is important in many areas of physics, from magnetic resonance to quantum information processing. Theoretical description of the spin-bath decoherence is a rather old problem, and many approaches of different degree of sophistication have been developed for different interesting solid-state systems, starting from early days of NMR/ESR theory (see e.g. Refs. S3, S4), till very recently (see e.g. Refs. 3–10 of the main text). All these theories

involve a trade-off between quantitative rigour and qualitative understanding. Some theories use simplified phenomenological treatments and involve assumptions about the system's behavior, but allow all calculations to be performed analytically, and give a very clear (although crude) qualitative picture of the underlying physics. Other theories use more detailed numerical simulations, with fewer (or no) assumptions, and gain quantitative rigour at the expense of being much less clear. In the present work, we use two theoretical approaches, located at the opposite ends of this dilemma. First, we use a simple phenomenological model which allows for a completely analytical treatment, and provides qualitative understanding of experiments. Second, we use direct numerical simulations, starting straight from the relevant micoroscopic Hamiltonians; these simulations give much less qualitative insight, but involve absolutely no assumption about the behaviour of the system. The agreement between both approaches and the experimental results allows us to achieve both goals: to gain qualitative insights into the dynamics of decoherence of an NV center, and, at the same time, to make sure that our qualitative physical picture is correct.

Below, in Sections 3–4, we explain in detail the microscopic structure and derivation of the Hamiltonians for the NV and P1 centers. Explanation of a simplified analytical model for the bath of P1 centers, and the analytical results are given in Sec. 5. The details of numerical simulations are given in Sec. 6.

For convenience, everywhere below we take the Planck's constant $\hbar = 1$, and express the energy quantities in frequency units.

3 Hamiltonian of a single NV center

Along with the single-axis anisotropy mentioned above, another important interaction is the hyperfine coupling at the NV site, i.e. the coupling between the electron spin $S_0 = 1$ and the nuclear spin ^{14}N of the NV center (denoted below as I_0). The relevant hyperfine Hamiltonian is deduced from the experimental measurements in Refs. S7, S8:

$$H_{hf}^0 = A_0 S_0^z I_0^z + A_1 (S_0^x I_0^x + S_0^y I_0^y) - P_0 (I_0^z)^2. \tag{S1}$$

where $A_0 = 2.3$ MHz, $A_1 = 2.1$ MHz, and $P_0 = -5.1$ MHz. Also, external magnetic fields can be applied to the system: (1) a static magnetic field B along the z-axis ($[111]$ direction), and/or (2) an oscillating field H_R with frequency ω can be applied to the NV center along the x-axis, either in order to study Rabi oscillations, or to implement the π- and $\pi/2$-pulses in the Ramsey and Hahn spin echo experiments. Thus, the relevant part of the NV center Hamiltonian is

$$H_S = D(S_0^z)^2 + A_0 S_0^z I_0^z + A_1 (S_0^x I_0^x + S_0^y I_0^y) - P_0 (I_0^z)^2 + g_0 \mu_B B S_0^z + g_0 \mu_B H_R S_0^x \cos \omega t, \tag{S2}$$

where $g_0 = 2$ is the Landé factor of the NV center, and μ_B is Bohr's magneton. This Hamiltonian is complex, and inconvenient for numerical simulations, as it contains large energy scales: D and, in case of large magnetic field, $g_0 \mu_B B$. Significant simplification can be achieved by

going to the interaction representation, which excludes the large terms from the Hamiltonian (S2), and treating the remaining terms perturbatively.

Below, we perform this simplification for two experimentally relevant situations: zero magnetic field $B = 0$, and large magnetic field $B = 740$ G. In NMR/ESR language, we apply the standard procedure of rotating-frame transformation and omission of the non-secular (explicitly time-dependent) terms (*S10*).

3.1 Zero magnetic field, $B = 0$

At zero magnetic field, we eliminate the first term by applying a unitary transformation $U_1 = \exp\left[-iD(S_0^z)^2 t\right] = 1 + (S_0^z)^2[\exp(-iDt) - 1]$ to the Hamiltonian (S2), treating the term $D(S_0^z)^2$ as a zero-order Hamiltonian, and everything else as a perturbation. In this way, the terms containing the operators S_0^x and S_0^y become time-dependent, oscillating with the frequency D. Due to these oscillations, for instance, the third term in (S2) is averaged out: its time-average value is zero, so it gives no contribution in the first-order approximation. In the second order, the effect of this term is twofold. Firstly, it mixes the state $|m_S = 0\rangle$ with $|m_S = \pm 1\rangle$ and slightly renormalizes their energies. These effects are small ($A_1/D \sim 10^{-3}$), and can be neglected: e.g., the energy corrections are of order of $A_1^2/D \sim 1.5$ kHz, and they can be visible only at timescales of few milliseconds, much larger than the relevant experimental timescales (few microseconds). Secondly, the term $A_1(S_0^x I_0^x + S_0^y I_0^y)$ can strongly mix the states $|m_S = +1\rangle$ and $|m_S = -1\rangle$, since they are degenerate in zeroth order. However, this effect is also too weak, and any external field larger than $A_1^2/D \sim 10^{-3}$ G already destroys it (this field can come, for instance, from interaction with the bath, which is of order of 0.1 G). Finally, we note that since this term does not affect the electron spin S_0, it also does not affect the nuclear spin I_0, because the flip-flop processes involve both S_0 and I_0. The conclusion is that the third term in (S2) can be safely dropped. The nuclear quadrupolar term $P(I_0^z)^2$ then becomes just a constant, and can also be ignored.

However, the last term in the Hamiltonian (S2) requires more care: it is already explicitly time-dependent, and after the unitary transformation U_1, its dependence on time has the form of either $\exp(iDt)\cos\omega t$ or $\exp(-iDt)\cos\omega t$, depending on the position in the S_0^x matrix. In zero-magnetic field experiments, the frequency of the oscillating field is $\omega = D$, so that the terms $\exp(\pm iDt)\cos\omega t$ contain both non-oscillating part $1/2$ and the part oscillating with the frequency $2D$. The oscillating part has negligible effect: all considerations of the previous paragraph can be applied here with minor modifications. Thus, we retain only the non-oscillating (secular) part, and the Hamiltonian of the NV center then becomes

$$H_S = A_0 S_0^z I_0^z + (1/2) g_0 \mu_B H_R S_0^x. \tag{S3}$$

Note that the last term, which describes the action of the oscillating driving field, excites both transitions $|m_S = 0\rangle \leftrightarrow |m_S = 1\rangle$ and $|m_S = 0\rangle \leftrightarrow |m_S = -1\rangle$.

Finally, we note that in this work, we do not excite the nuclear spin of the NV center, and the intrinsic relaxation time (due to e.g. spin-phonon coupling) of the spin I_0 is of order

of milliseconds. Thus, for a single experimental run, the nuclear spin is frozen, and I_0^z is the constant of motion. Then, the nuclear spin I_0 just creates an additional static magnetic field along the z-axis (equal to $\pm A_0$ or zero, depending on m_I, where $m_I = 0, \pm 1$ denotes the eigenstates of I_0^z). However, between different experimental runs, the nuclear spin has enough time to switch to a state with another m_I. Thus, in order to calculate the experimentally observable population $p_0(t)$ of the state $m_S = 0$, we need to perform calculations for different m_I, and average the result.

3.2 Large magnetic field, $B = 740$ G

If the magnetic field B is large, then the transitions $|m_S = 0\rangle \leftrightarrow |m_S = 1\rangle$ and $|m_S = 0\rangle \leftrightarrow |m_S = -1\rangle$ have very different frequencies: $D + g_0\mu_B B$ for the first transition, and $D - g_0\mu_B B$ for the second one. In experiments, the driving field frequency ω is set to excite only the second transition, $\omega = D - g_0\mu_B B$, so that the state $|m_S = +1\rangle$ is not affected at all. In this case, the NV center can be described in terms of a fictituous spin $s_0 = 1/2$, with the state $|\uparrow\rangle$ of s_0 corresponding to $|m_S = 0\rangle$, and the state $|\downarrow\rangle$ of s_0 corresponding to $|m_S = -1\rangle$. By projecting the full Hamiltonian (S2) onto the subspace spanned by the levels $|m_S = 0\rangle$ and $|m_S = -1\rangle$, an effective Hamiltonian for the spin s_0 is obtained:

$$H_S = A_0 s_0^z I_0^z + (1/\sqrt{2}) g_0\mu_B H_R s_0^x. \tag{S4}$$

where the non-secular terms are excluded in the same way as in Sec. 3.1 (all considerations of that section are applicable here with minor modifications).

4 Hamiltonian of the bath, and coupling of an NV center to the bath

The bath is made of nitrogen atoms (P1 centers, Ref. S2), each having an unpaired electron with the spin $S_k = 1/2$ and a ^{14}N nuclear spin $I_k = 1$. The hyperfine coupling between S_k and I_k is rather strong (around 100 MHz), and should be taken into account.

4.1 Hamiltonian of a single P1 center

In order to describe the role of the hyperfine coupling, we need to consider the microscopic structure of a P1 center. At every P1 center, the unpaired electron is shared by the nitrogen atom and the neighboring carbon atom. Such a delocalization of the electron is accompanied by the Jahn-Teller elongation of the corresponding carbon — nitrogen bond. For every nitrogen, there are four equivalent neighboring carbons, so the electron can be delocalized along one of four axes: $[111]$, $[\bar{1}11]$, $[1\bar{1}1]$, and $[11\bar{1}]$. Correspondingly, there are four types of P1 centers. For a given P1 center, let us introduce a local coordinate system (X, Y, Z), with the Z-axis coinciding

with the delocalization axis of this P1 centers. For one type of center, with the delocalization axis $[111]$, the local coordinates (X, Y, Z) coincide with the laboratory coordinates (x, y, z). For three other types, (X, Y, Z) differ from (x, y, z) by a $90°$- or a $180°$-rotation around the c-axis of the crystal. In the local coordinate frame, the hyperfine Hamiltonian of a single P1 center is of single-axis type (*S2, S9*):

$$H_L = A_Z I_k^Z S_k^Z + A_X (I_k^X S_k^X + I_k^Y S_k^Y) - P (I_k^Z)^2 \tag{S5}$$

where (I_k^X, I_k^Y, I_k^Z) are the operators of the k-th nuclear spin in the local coordinate frame, (S_k^X, S_k^Y, S_k^Z) are the operators of the k-th nitrogen electron spin in the local coordinate frame, and the hyperfine and quadrupole parameters are known (*S2, S9*): $A_Z = 114$ MHz, $A_X = 81.3$ MHz, and $P = -4$ MHz. Note that the electron spin $S_k = 1/2$ of a P1 center has no anisotropy, so that the simplifications of Sec. 3.1 can not be used here.

It is important to note that the delocalization axis of a given P1 center can change in time, switching from one possible direction to another. At room temperatures, the time between such switches is much longer than the characteristic time of a single experimental run. On the other hand, during the whole experiment (which includes 10^5 single runs), the delocalization axis of a given nitrogen can switch several times. Thus, in calculations, we should consider the axis direction as static, but, in the end, average over all possible directions of the delocalization axis.

The Hamiltonian (S5) has three doubly degenerate eigenenergies: $E_0 = 0$ (corresponding eigenfunctions will be denoted as $|\phi_0, +\rangle$ and $|\phi_0, -\rangle$), $E_1 = 130$ MHz (with eigenfunctions $|\phi_1, +\rangle$ and $|\phi_1, -\rangle$), and $E_2 = 149$ MHz (eigenfunctions $|\phi_2, +\rangle$ and $|\phi_2, -\rangle$). Each pair of states $|\phi_F, \pm\rangle$ (where $F = 0, 1, 2$) represents a Kramers doublet, and the degeneracy is caused by the time-reversal symmetry of the Hamiltonian (S5). Note that the energy difference between these doubly degenerate subspaces is much larger than dipolar coupling to the NV center and to other P1 centers; this fact will be used below.

The eigenfunctions $|\phi_F, \pm\rangle$ are the entangled states of the electron and the nuclear spin of a P1 center. For instance, for a type-1 center, these functions can be expressed in the basis $|S_k^z; I_k^z\rangle$ as follows:

$$\begin{aligned}
|\phi_{0,-}\rangle &= -p|1/2; 0\rangle + q|-1/2; 1\rangle, \quad |\phi_{0,+}\rangle = -q|1/2; -1\rangle + p|-1/2; 0\rangle; \\
|\phi_{1,-}\rangle &= p|1/2; -1\rangle + q|-1/2; 0\rangle, \quad |\phi_{1,+}\rangle = -q|1/2; 0\rangle - p|-1/2; 1\rangle; \\
|\phi_{2,-}\rangle &= |-1/2; -1\rangle, \quad |\phi_{2,+}\rangle = |1/2; 1\rangle;
\end{aligned} \tag{S6}$$

where $p = 0.515$ and $q = 0.857$. Note that p and q are close to $\sqrt{1/3}$ and $\sqrt{2/3}$, correspondingly; this is due to fact that the values of A_X and A_Z are close to each other, and the value of P is small. If A_X and A_Z were exactly equal and P were zero, then the hyperfine coupling would be isotropic, and the eigenstates of the hyperfine Hamiltonian would have a well-defined total spin J_k: there would be two states with $J_k = 1/2$, and four states with $J_k = 3/2$, and the values of p and q then would be equal to the corresponding Clebsch-Gordan coefficients $\sqrt{1/3}$ and $\sqrt{2/3}$.

At large magnetic field, the Zeeman term $g\mu_B B S_k^z$ has to be added to the Hamiltonian (S5), where $g = 2$ is the Landé factor of the electron spin of the P1 center; note that the field is directed along the z-axis of laboratory frame, not Z-axis of the local frame. Due to the large field $B = 740$ G, the Hamiltonian can be simplified using the arguments similar to those of Sec. 3.1; the resulting Hamiltonian is

$$H_L = g\mu_B B S_k^z + A_1 S_k^z I_k^z \tag{S7}$$

where $A_1 = 114$ MHz for the P1 centers of the type 1 (with the delocalization axis $[111]$), and $A_1 = 86$ MHz for the P1 centers of the other types (with the delocalization axis directed along $[\bar{1}11]$, $[1\bar{1}1]$, or $[11\bar{1}]$).

4.2 Coupling between P1 centers and NV center

The coupling between the NV center and the nitrogen atoms is of dipolar origin. Assuming that the NV center is located at the origin of the laboratory frame, it is:

$$H_{SB} = \sum_k \frac{g_0 g \mu_B^2}{r_k^3} \left[\mathbf{S}_0 \mathbf{S}_k - 3(\mathbf{S}_0 \mathbf{n}_k)(\mathbf{S}_k \mathbf{n}_k)\right] \tag{S8}$$

where $\mathbf{r}_k$ is the radius-vector of the k-th nitrogen atom, $r_k = |\mathbf{r}_k|$, and $\mathbf{n}_k = \mathbf{r}_k / r_k$. Due to strong anisotropy of the NV center, this form can be simplified using the reasoning of Sec. 3.1.

4.2.1 Zero magnetic field

For the case of zero magnetic field, applying the unitary transformation U_1 (see Sec. 3.1), we obtain:

$$H_{SB} = \sum_k a_k S_0^z \left[S_k^z - 3 n_k^z (\mathbf{S}_k \mathbf{n}_k)\right], \tag{S9}$$

where $a_k = g_0 g \mu_B^2 / r_k^3$. However, simplicity of this expression is illusory: the local Hamiltonian of the P1 center (S5) is rather complex.

To simplify matters, we note that the typical value of a_k is of order of 0.5 MHz or smaller, so that this coupling Hamiltonian can be treated as a perturbation, with H_L of Eq. S5 being the zeroth-order Hamiltonian. Thus, we can take into account only those matrix elements of H_{SB} which connect the states of H_L with equal energies, i.e. only the elements $\langle \phi_{F,\pm} | H_{SB} | \phi_{F,\pm} \rangle$ where $F = 0$, 1, or 2, and neglect all other elements. In this way, instead of complex 6-level Hilbert space of a P1 center, we have three uncoupled 2-level subspaces (indexed by $F = 0$, 1, 2). Each 2-level subspace can be described as a pseudo-spin-1/2 system, with the pseudo-spin operators $S_k'^{\alpha}$ ($\alpha = x, y, z$), where the state $|\phi_{F,+}\rangle$ corresponds to the state $|\uparrow\rangle$ of the pseudo-spin and the state $|\phi_{F,-}\rangle$ corresponds to the state $|\downarrow\rangle$. For instance, for a P1 center of type 1, up to possible unitary transformation, the operators $S_k^{x,y,z}$ of the P1 center within these subspaces

have the following nonzero elements:

$$\begin{aligned}\langle\phi_{F,+}|S_k^z|\phi_{F,+}\rangle &= -\langle\phi_{F,-}|S_k^z|\phi_{F,-}\rangle = r_z \\ \langle\phi_{F,+}|S_k^x|\phi_{F,-}\rangle &= \langle\phi_{F,-}|S_k^x|\phi_{F,+}\rangle = r_x \\ \langle\phi_{F,+}|S_k^y|\phi_{F,-}\rangle &= -\langle\phi_{F,-}|S_k^y|\phi_{F,+}\rangle = r_y\end{aligned} \tag{S10}$$

where $r_x = 0.133$, $r_y = i \cdot 0.133$, $r_z = 0.234$ for $F = 0$; $r_x = 0.367$, $r_y = i \cdot 0.367$, $r_z = 0.234$ for $F = 1$; and $r_x = r_y = 0$, $r_z = 0.5$ for $F = 2$. Thus, for the type-1 P1 center with fixed F, we can simply replace S_k^α by $2r_\alpha S_k'^\alpha$ ($\alpha = x, y, z$), where the operators $S_k'^\alpha$ are unitarily equivalent to S_k^α. The matrix elements for other types of P1 centers (with other delocalization axes) can be obtained by appropriate rotations around the c-axis of the crystal.

Since the pseudo-spin operators $S_k'^\alpha$ ($\alpha = x, y, z$) are related to the spin operators S_k^α ($\alpha = x, y, z$) via simple unitary transformation, the Hamiltonian of interaction between the NV center and a nitrogen atom can be written as

$$H_{SB} = \sum_{k,\alpha} a'_{k,\alpha} S_0^z S_k'^\alpha \tag{S11}$$

where the new coupling parameters $a'_{k,\alpha}$ are linearly related to the original couplings a_k of the Hamiltonian (S9); for instance, for a type-1 P1 center, $a'_{k,\alpha} = 2a_k r_\alpha(\delta_{\alpha,z} - 3n_k^z n_k^\alpha)$, where $\delta_{\alpha,z}$ is the Kronecker's symbol. By an appropriate unitary transform, this Hamiltonian can be rewritten in the simple form

$$H_{SB} = \sum_k \tilde{a}_k S_0^z \tilde{S}_k^z, \tag{S12}$$

where $\tilde{S}_k^z$ is unitarily equivalent to the "original" spin operator S_k^z, and the renormalized coupling coefficients $\tilde{a}_k = \sqrt{(a'_{k,x})^2 + (a'_{k,y})^2 + (a'_{k,z})^2}$ are proportional to a_k of the "original" Hamiltonian (S9); the proportionality coefficient depends on $\mathbf{n}_k$, value of F, and type of the P1 center (direction of its delocalization axis).

4.2.2 Large magnetic field

For large magnetic field, the coupling Hamiltonian is simplified easily. Neither of the spins S_0 or S_k can be flipped due to dipolar interactions, since the mismatch in energies between different states of S_0 or S_k is very large. Formally, we take the Zeeman term (for S_k) and the Zeeman-plus-anisotropy term (for S_0) as a zeroth-order Hamiltonian, and omit the non-secular terms from the coupling Hamiltonian (S9). In terms of the pseudo-spin $s_0 = 1/2$ (see Sec. 3.2), we obtain:

$$H_{SB} = \sum_k a_k[1 - 3(n_k^z)^2](s_0^z - 1/2)S_k^z = \sum_k c_k s_0^z S_k^z - (1/2)\sum_k c_k S_k^z, \tag{S13}$$

where $a_k = g_0 g\mu_B^2/r_k^3$, and $c_k = a_k[1-3(n_k^z)^2]$. Note that the last term renormalizes the internal Hamiltonian of the bath.

4.3 Dipolar coupling between different P1 centers

The coupling between different P1 centers is important since it gives rise to the internal dynamics of the bath. The Hamiltonian of a pair of dipolarly coupled nitrogen atoms is

$$H_{jk} = H_{L,j} + H_{L,k} + H_{dip,jk} \tag{S14}$$

$$H_{dip,jk} = g^2\mu_B^2 \frac{1}{r_{jk}^3}\left[\mathbf{S}_j\mathbf{S}_k - 3(\mathbf{S}_j\mathbf{n}_{jk})(\mathbf{S}_k\mathbf{n}_{jk})\right], \tag{S15}$$

where $\mathbf{S}_j$ is the electron spin of the j-th nitrogen, $\mathbf{S}_k$ is the electron spin of the k-th nitrogen, and $\mathbf{r}_{jk}$ is the radius-vector connecting the two nitrogens ($r_{jk} = |\mathbf{r}_{jk}|$, and $\mathbf{n}_{jk} = \mathbf{r}_{jk}/r_{jk}$). The local Hamiltonians $H_{L,j}$ and $H_{L,k}$ have the form (S5) or (S7), depending on magnetic field; note that the local coordinate frames (X, Y, Z) for the centers j and k may be different, depending on how their delocalization axes are oriented with respect to the lab frame. The characteristic value of such an intra-bath coupling is of the same order as the coupling between the NV center and the P1 centers (i.e., of order of 0.5 MHz).

At zero magnetic field, the dipolar interaction leads to both single-spin flips and pairwise flip-flops. E.g., if k-th spin is in the state $|\phi_{F,+}\rangle$ with $F = 1$ or $F = 2$, the effect of the term $S_j^z S_k^x$ in Eq. S14 is to change the k-th spin state from $|\phi_{F,+}\rangle$ to $|\phi_{F,-}\rangle$, since such a transition does not change the energy and has a nonzero matrix element. In so doing, the state of the j-th spin may remain unchanged: e.g., if the j-th spin belongs to a type-1 nitrogen center, then the action of S_j^z does not lead to a flip of j-th spin. On the other hand, if the k-th spin is in the state $|\phi_{3,\pm}\rangle$, the only way for it to flip is to make a transition to another state, e.g. with $F = 1$ (or $F = 2$). Such a transition changes the energy of the k-th spin; the energy conservation then requires that the j-th spin is in the state with $F = 1$ (or $F = 2$). Thus, majority of states of the P1 centers may flip very fast, while others preserve their state for long time, being pretty much static.

At large magnetic field, the situation changes. The single-spin flips are prohibited: they do not conserve energy. But even two-spin flip-flop processes are strongly suppressed. First, the local hyperfine interaction at a P1 site (see Eq. S7) creates an extra field ($+A_1$, $-A_1$, or zero), which is determined by the nitrogen's nuclear spin I_k^z; the magnitude of this field also depends on the type of the P1 center, since A_1 is different for the centers of type 1 and the centers of type 2, 3, and 4. Thus, for the j-th bath spin to flip, it is necessary that the k-th spin has the value of I_k^z equal to I_j^z, and that these two centers have the same A_1. Second, at large magnetic field, the internal Hamiltonian of the bath is renormalized, see Eq. S13, and different extra fields, created by the NV center, act on different P1 centers. As a result, the dynamics of the bath spins at large magnetic field is strongly suppressed, and only a few spins can change their orientation with time.

5 Analytical theory for decoherence dynamics of an NV center

Exact microscopic calculations, based directly on Eqs. S3, S12, and S14 for zero magnetic field (or Eqs. S4, S13, and S14 for large magnetic field) are too complex for analytics, and we use numerical simulations described in Sec. 6. For analytical treatment, a simplified model is needed. Below, we provide justification, and describe such a model. We consider the relevant experiments (decay of Ramsey fringes, damping of Hahn spin echo, and decay of Rabi oscillations), and show how our analytical model helps in understanding the results.

5.1 Description of the phenomenological model: justification and qualitative conclusions

We start from summarizing the results of the microscopic considerations given above. For zero magnetic field, the Hamiltonian of the NV center coupled to the bath of nitrogen atoms, has a form

$$H = B_z S_0^z + h_x S_0^x + H_B \tag{S16}$$

where H_B is the internal Hamiltonian of the bath (it includes both local Hamiltonians of the P1 centers and the dipolar interactions between them), $h_x = (1/2) g_0 \mu_B H_R$, and $B_z = A_0 I_0^z + \tilde{a}_k \tilde{S}_k^z$. For large magnetic field, the relevant Hamiltonian has a similar form

$$H = B_z s_0^z + h_x s_0^x + H_B \tag{S17}$$

where $h_x = (1/\sqrt{2}) g_0 \mu_B H_R$, and $B_z = A_0 I_0^z + c_k S_k^z$. Aside from the parameter values, the only difference between these two Hamiltonians is that the central spin $S_0 = 1$ at zero magnetic field while $s_0 = 1/2$ at large magnetic field.

If we omit for a moment the bath's internal Hamiltonian H_B, the exact solution of the problem can be obtained by purely analytical means for both zero and large magnetic field. It is important to recognize that I_0^z is a constant of motion, and, if $H_B = 0$, S_k^z (or $\tilde{S}_k^z$) are the constants of motion, too. Thus, if the k-th bath spin was initially in the state $|\uparrow\rangle$, then it will remain in this state, and the operator S_k^z in this case can be replaced by a c-number equal to $\langle\uparrow |S_k^z| \uparrow\rangle = 1/2$. Thus, B_z in Eqs. S16 and S17 can be treated simply as some real number, whose value depends upon the specific initial state of the bath. Finally, we must average over all possible initial states of the bath; all these states are equally probable (at room temperature). The corresponding distribution $P(B_z)$ of the values of B_z is given by the central limit theorem of the probability theory: it is a Gaussian distribution, with the mean equal to $A_0 I_0^z$ (i.e., to $+A_0$, $-A_0$, or zero, with equal probability), and with the variance $b^2 = (1/4) \sum_k c_k^2$ (or, for zero magnetic field, $\tilde{b}^2 = (1/4) \sum_k \tilde{a}_k^2$). Thus, for $H_B = 0$, it is a rigorously justified step to replace the action of the static bath by the action of the static Gaussian random field B_z.

In reality, when the internal bath dynamics determined by H_B is not negligible, the bath spins can change its orientation (flip), and S_k^z is not an integral of motion anymore. In order

to deal with this complication, we make an important approximation: we treat the bath in a mean-field manner, assuming that the influence of the bath spins on the NV center can still be approximated as the action of some random field B_z, which now may depend on time. This mean-field approximation is a standard (and probably, the most transparent) way for describing a wide variety of NMR/ESR-like experiments, successfully used since the 1950s (*S3, S4*) until present times (*S5*). Of course, applicability of the mean-field approximation requires an independent confirmation. In our case, the validity of the model is confirmed by direct microscopic numerical simulations, and by very good agreement with the experimental results. This is also the reason why, in this work, we do not use more sophisticated approaches, which, for instance, take into account two-spin correlations inside the bath (*S5*). Such approaches are less qualitatively clear than the mean field, but, unlike direct numerical simulations, still need to invoke assumptions about the bath dynamics (e.g., that the 2-spin correlations are sufficient); checking validity of these assumptions and development of such theories for NV centers requires a separate detailed investigation.

In order to construct the correct model for the dynamics of the random field B_z, we recall (see Sec. 4.3) that the rate of flipping of a given nitrogen spin depends very strongly on the type of this nitrogen atom, on the value of the parameter F (for zero magnetic field) or the value of I_k^z of this atom (for large magnetic field), and on the state of its neighbors. Therefore, for some spins S_k^z can be well approximated as static, while for other spins this approximation is invalid. Moreover, whether S_k^z can be approximated as static depends on the coupling of the k-th spin to the NV spin. This fact, derived during early days of the NMR/ESR theory (*S6*), can be qualitatively explained as follows (for formal derivation, see the original work, Ref. S6). Let us assume that the characteristic time for a flip of a given spin is τ_c, and the coupling constant is Δ_k. This spin imposes a random time-varying field on the NV center, so that, after some time t, the state $|m_S = +1\rangle$ of the NV center acquires some phase β, while the state $|m_S = -1\rangle$ acquires a phase $-\beta$. The quantity determining the decoherence rate is the average of $\exp(i\beta)$ over all possible realizations of the random field; in Ref. S6, this average is denoted as $v_k(t)$. The value of v_k depends on whether $\Delta_k\tau_c \gg 1$ or $\Delta_k\tau_c \ll 1$: in the former case, the k-th bath spin is practically static, and $v_k(t) \approx 1 - \Delta_k^2 t^2/2$, while in the latter case, the k-th spin is in the regime of motional narrowing (*S3, S4*) with $v_k(t) \approx \exp(-\Delta_k^2\tau_c t/2)$.

In a real bath, there are many spins with different Δ_k and different τ_c. We simplify the situation in the spirit of Ref. S6, assuming that the spins with $\Delta_k\tau_c > 1$ can be treated as static, while the spins with $\Delta_k\tau_c < 1$ can be treated as being in the regime of complete motional narrowing. Thus, the mean field B_z acting on the NV center contains two components: one is a static random Gaussian field with the mean $A_0 I_0^z$ and the variance b^2 (or $\tilde{b}^2$, for zero magnetic field), and the other is the fast Gaussian random field with the mean zero, variance b_1^2 (or $\tilde{b}_1^2$) and correlation time τ_c such that $b_1\tau_c \ll 1$ (or, for zero magnetic field, $\tilde{b}_1\tilde{\tau}_c \ll 1$).

Based on our knowledge of microscopic Hamiltonians (see discussions in this Section above and Sec. 4.3), we can make some qualitative conclusions about expected experimental results. At large magnetic field, in comparison with the zero-magnetic field case, the majority of bath spins are difficult to flip, and the spin correlation time τ_c at large magnetic field should be larger

than the correlation time $\tilde{\tau}_c$ at zero magnetic field. Moreover, the coupling coefficients $\tilde{a}_k$ at zero magnetic field are, in general, smaller than the coupling coefficients c_k at large magnetic field. Indeed, at zero magnetic field, due to the hyperfine coupling between the electron and nuclear spins of a given nitrogen atom, the matrix elements of the operators $S_k^{x,y,z}$ are significantly smaller than 1/2, see Eqs. S10. At large magnetic field, no such renormalization exist, and the coupling coefficients c_k are, on average, larger than $\tilde{a}_k$. Thus, at large magnetic field, more spins satisfy the inequality $\Delta_k \tau_c > 1$, i.e., at large magnetic field the majority of spins is static. Therefore, the value of b should be larger than $\tilde{b}$, while b_1 should be smaller than $\tilde{b}_1$. This is exactly what we observe in experiments. Furthermore, we expect that, qualitatively, the Ramsey fringes decay should be faster at large magnetic fields (where the static component of the bath field is larger), while the decay of Hahn spin echo should be faster at zero magnetic field (where the dynamic component of the bath field is larger). Again, this is what we observe in experiments.

Here, we do not go beyond these qualitative conclusions: development of a detailed microscopic theory for the bath parameters (b and $\tilde{b}$, b_1 and $\tilde{b}_1$, etc.) is not a main topic of our work. Such a theory would involve many complications: the bath spins in our case are complex entities, the interaction coefficients have complex dependence on the internal state of the nitrogen atoms and on the position of a given nitrogen atom, etc. (e.g., note that in the work *S6* the dependence of Δ_k on the direction of the vector $\mathbf{n}_k$ is neglected). A detailed theory of this kind has been developed, e.g., for decoherence of a spin-1/2 P donor by a bath of ^{29}Si spins 1/2 (*S5*), but even for that simpler bath the description is very complex. Development of similar description for NV centers would require a separate investigation. Therefore, everywhere below we treat the bath parameters as phenomenological quantities, which are extracted from experiments.

5.2 Analytical solution for the Ramsey fringes experiments

We first consider the decay of Ramsey fringes; this experiment is equivalent to the free induction decay in NMR/ESR. The NV center is prepared in the state $|m_S = 0\rangle$, and a $\pi/2$ pulse is applied along the x-axis. We assume that the $\pi/2$ rotation is ideal (the width of the pulse is of order of 10 ns, and the influence of the field B_z during this interval can be neglected). At zero magnetic field, the initial state is

$$|\psi_0\rangle = -\frac{i}{\sqrt{2}} \left(|m_S = 1\rangle + |m_S = -1\rangle \right), \tag{S18}$$

In the absence of driving ($h_x = 0$), the evolution of this state is easy to calculate: after time t, the state $|m_S = 1\rangle$ acquires a phase $\beta = \int_0^t B_z(s) ds$, while the state state $|m_S = -1\rangle$ acquires a phase $-\beta$. Then, another $\pi/2$ pulse is applied, and the population $p_0(t)$ of the state $|m_S = 0\rangle$ is measured, which is equal to $p_0(t) = (1 + \cos 2\beta)/2$; this value should be averaged over all possible β to give the experimentally detected average value $\langle p_0(t) \rangle$. In our model, B_z is a sum of two components, static B_z^s and dynamic $B_z^d(t)$, and their contributions to β are additive.

Therefore, we can first perform averaging over the static component, obtaining

$$\langle p_0(t)\rangle^s = \frac{1}{2} + \frac{1}{6}\left[1 + 2\cos 2A_0 t\right]\exp\left(-2\tilde{b}^2 t^2\right), \tag{S19}$$

where $\langle\cdot\rangle^s$ reminds that an averaging over $B_z^d(t)$ still should be performed. For large magnetic field, after the $\pi/2$ pulse, the state of the NV center is $(1/\sqrt{2})[|m_S = 0\rangle - i|m_S = -1\rangle]$. The calculations of $\langle p_0(t)\rangle^s$ can be done in a similar way, and the answer is:

$$\langle p_0(t)\rangle^s = \frac{1}{2} - \frac{1}{6}\left[1 + 2\cos A_0 t\right]\exp\left(-\tilde{b}^2 t^2/2\right). \tag{S20}$$

Note that for zero magnetic field, $\langle p_0(0)\rangle = 1$, since two subsequent $\pi/2$ pulses bring the state $|m_S = 0\rangle$ back to $|m_S = 0\rangle$, while for large magnetic field, two $\pi/2$ pulses transfer $|m_S = 0\rangle$ to $|m_S = -1\rangle$. The free induction decay (FID) given by Eqs. S19 and S20 has a Gaussian form $\exp\left(-t^2\right)$.

Now, we should perform an average over the dynamic component $B_z^d(t)$. This calculation is a part of standard NMR/ESR theory (*S3, S4*). For our problem, it can be shown that the averaging over $B_z^d(t)$ leads simply to multiplying the $\langle p_0(t)\rangle^s$ by a factor $\exp\left(-b_1^2\tau_c t/2\right)$ (or $\exp\left(-\tilde{b}_1^2\tilde{\tau}_c t/2\right)$). In the next subsection, we show that this is exactly the factor which determines the attenuation of the Hahn spin echo. Thus, expressing the decay of Ramsey fringes in terms of experimentally measured quantities, we have:

$$\langle p_0(t)\rangle = \frac{1}{2} + \frac{1}{6}\left[1 + 2\cos 2A_0 t\right]\exp\left[-2\tilde{b}^2 t^2\right]\exp\left(-t/\tilde{T}_2\right), \tag{S21}$$

for zero magnetic field, where $\tilde{T}_2$ denotes the decay time of the Hahn spin echo at zero magnetic field, and

$$\langle p_0(t)\rangle = \frac{1}{2} - \frac{1}{6}\left[1 + 2\cos A_0 t\right]\exp\left(-\tilde{b}^2 t^2/2\right)\exp\left(-t/T_2\right), \tag{S22}$$

for large magnetic fields, where T_2 is the decay time of the Hahn spin echo at large magnetic field.

5.3 Analytical results for Hahn spin echo decay

In the Hahn spin echo experiments, after applying the first $\pi/2$ pulse, we let the system evolve during the time interval τ, then apply the π pulse, wait for another time τ, and then apply the second $\pi/2$ pulse followed by the readout of $p_0(t)$. To analyze the Hahn spin echo theoretically, we note that during the intervals of free evolution between the pulses, the contributions to the phase β from B_z^s and B_z^d are additive, and can be analyzed separately. The effect of the static component is removed completely by the π pulse: the phase acquired due to B_z^s during the first interval τ is equal in magnitude, and opposite in sign, to the phase acquired due to B_z^s during the second interval τ.

Calculation of the effect of the dynamic component is also a standard part of NMR/ESR theory (*S3,S4*), and the answer is known: for the extreme motional narrowing regime, the decay of the Hahn spin echo is the same as the free induction decay (Ramsey fringes decay); denoting $t = 2\tau$, we obtain:

$$\langle p_0(t)\rangle = \frac{1}{2} + \exp\left(-\tilde{b}_1^2\tilde{\tau}_c t/2\right) = \frac{1}{2} + \exp\left(-t/\tilde{T}_2\right), \tag{S23}$$

for the zero magnetic field, and

$$\langle p_0(t)\rangle = \frac{1}{2} + \exp\left(-b_1^2\tau_c t/2\right) = \frac{1}{2} + \exp\left(-t/T_2\right), \tag{S24}$$

for large magnetic field. Indeed, in the motional narrowing regime, the bath fluctuations are fast, and the effect of the π pulse is quickly forgotten. Note that the measurements of the Ramsey fringes and Hahn spin echo decay do not allow reliable determination of both b_1 and τ_c (or $\tilde{b}_1$ and $\tilde{\tau}_c$): only their combination $b_1^2\tau_c$ determines the observable quantity T_2.

5.4 Rabi oscillations

Theoretical analysis of the Rabi oscillations is facilitated if performed in the rotating frame, which rotates with the frequency of the driving field H_R; in this way, the NV center Hamiltonian is static, see Sec. 3.1 and 3.2. Furthermore, in order to observe well-defined Rabi oscillations, a rather large driving field H_R is needed: otherwise, the decay time of the oscillations will be of the same order as an oscillation period. Thus, we perform analysis assuming that $h_x \gg B_z$ and $h_x\tau_c \gg 1$. These assumptions are not unavoidable: it is possible also to study analytically other situations with slowly decaying oscillations, but the results of different calculations agree with each other, while the approximation of large h_x allows to give a clear qualitative picture of underlying physics.

First, we note that, for the purposes of the present work, the influence of the dynamical component of B_z can be neglected. Qualitatively, it is a very natural result: the Rabi rotation of the spin S_0 around h_x is the fastest process, which averages out the field B_z. If the dynamic part of B_z is sufficiently slow, much slower than the rotation of S_0 (i.e., $h_x\tau_c \gg 1$), then it just introduces an extra averaging, which is small in comparison with the averaging due to fast Rabi rotation. This conjecture can be confirmed by explicit calculations within the random-field approximation (*S12*); neglecting the dynamic part of B_z is confirmed as a good approximation by the agreement with the numerical simulations (which do not neglect the bath dynamics) and with the experimental results.

At zero magnetic field, the relevant Hamiltonian is

$$H = B_z S_0^z + h_x S_0^x \tag{S25}$$

with B_z being a static Gaussian field with mean $A_0 I_0^z$ and variance $\tilde{b}$. The time evolution operator for this Hamiltonian can be found exactly for any given B_z:

$$U = 1 + (\cos\Omega t - 1)\left[(2/3) + 2u_x u_z Q_0^{xz} + u_x^2 Q_0^{xx} + u_z^2 Q_0^{zz}\right] - i\left[u_x S_0^x + u_z S_0^z\right]\sin\Omega t, \tag{S26}$$

where $\Omega = \sqrt{B_z^2 + h_x^2}$, $u_x = h_x/\Omega$, $u_z = B_z/\Omega$, and $Q_0^{\alpha\beta} = (1/2)[S_0^\alpha S_0^\beta + S_0^\beta S_0^\alpha] - (2/3)\delta_{\alpha\beta}$ are the quadrupolar operators.

In the limit of $h_x \gg \tilde{b}$, for times larger than $\tilde{b}^{-1}$, one can show that it is sufficient to expand Ω up to second order in B_z/h_x, and neglect B_z everywhere else (i.e., take $u_z = 0$ and $u_x = 1$). The probability $p_0(t)$ then has a very simple form:

$$p_0(t) = \cos^2 \Omega t \tag{S27}$$

and should be averaged over all possible B_z, which has a distibution

$$P(B_z) = (1/3)(P_+ + P_- + P_0), \tag{S28}$$

where $P_{+,-,0}$ are all Gaussians with the variance $\tilde{b}$, and mean $+A_0$ for P_+, $-A_0$ for P_-, and zero for P_0. These three Gaussians correspond to $m_I = +1$, $m_I = -1$, and $m_I = 0$ respectively, and the average $\langle p_0(t)\rangle$ is an arithmetic average of three contributions. The contribution from $m_I = 0$ part is a slowly decaying phase-shifted oscillation:

$$\langle p_0(t)\rangle_0 = \frac{1}{2} + \frac{1}{2}\left[1 + 4\frac{b^4 t^2}{h_x^2}\right]^{-1/4} \cos\left(2h_x t + \phi\right) \tag{S29}$$

where the phase shift is $\phi = (1/2)\mathrm{arctan}(2b^2 t/h_x)$. Note that the decay at long times is of power-law form $\propto 1/\sqrt{t}$, and has noticeable amplitude even at very large times. Such an interesting decay has been noticed in earlier works (*S13*) (see also Refs. 8–10 of the main text), and signatures of this behavior have been recently observed in quantum dots (*S14*).

The contributions from the parts $m_I = +1$ and $m_I = -1$ are equal to each other, and have the form:

$$\begin{aligned} \langle p_0(t)\rangle_\pm &= \frac{1}{2} + (1+\xi^2)^{-1/4} \exp\left[-(1/2)v^2\xi^2/(1+\xi^2)\right] \cos\left[2h_x t + \Phi\right] \\ \Phi &= v^2\xi + \phi - (1/2)v^2\xi^3/(1+\xi^2) \end{aligned} \tag{S30}$$

where we introduced the "dimensionless time" $\xi = 2\tilde{b}^2 t/h_x$, the quantity $v = A_0/b$, and the phase $\phi = (1/2)\mathrm{arctan}\xi = (1/2)\mathrm{arctan}(2b^2 t/h_x)$ is the same as above.

Inspection of Eq. S30 shows that $\langle p_0(t)\rangle_\pm$ is a product of two decaying functions and one oscillating cosine with time-varying phase. One decaying function is the same power-law $1/\sqrt{t}$ decay (the term $(1+\xi^2)^{-1/4}$) which appeared in Eq. S29, and the other one is the exponent which saturates at $t \to \infty$ at the value $\exp(-v^2/2)$. At zero magnetic field, when $\tilde{b} \ll A_0$, the Eq. S30 is considerably simplified: in this case $v \gg 1$, and all terms which do not involve v (except for the large phase $2h_x t$) can be neglected. The result is a simple Gaussian decay of oscillations

$$\langle p_0(t)\rangle_\pm = \frac{1}{2} + \frac{1}{2}\exp\left[-2A_0^2\tilde{b}^2 t^2/h_x^2\right] \cos 2h_x t \tag{S31}$$

with the characteristic decay time $h_x/(A_0\tilde{b})$.

This result is very natural (see also Fig. 3 and accompanying part of the main text). For $m_I = 0$, the Rabi field h_x is perpendicular to the B_z field, and the fast rotation of S_0 around h_x completely averages out B_z in the first order. The effect of B_z is seen only in the second order (the decay time in Eq. S29 is of order of $\tilde{b}^2/h_x$), and this effect is small, leading to a slow power-law decay. For $m_I = \pm 1$, due to the finite mean $\pm A_0$, the Rabi field h_x is not exactly perpendicular to B_z, and the part of B_z which is not averaged by fast Rabi rotation leads to a standard Gaussian decay.

When we sum the contributions from all three values of m_I, an interesting effect takes place. The oscillations of $\langle p_0(t)\rangle_0$ decay very slowly, but have a time-varying phase, while the oscillations of $\langle p_0(t)\rangle_\pm$ decay rather fast. Thus, at some moment of time, the term $\langle p_0(t)\rangle_0$ can be equal to twice $\langle p_0(t)\rangle_\pm$ but have an opposite sign. In this case, the total $\langle p_0(t)\rangle$ would be equal to zero. Correspondingly, Rabi oscillations around that time would demonstrate a dip. Later, as $\langle p_0(t)\rangle_\pm$ decay further, this dip would disappear, reviving the Rabi oscillations.

The model has two free parameters for the Rabi oscillations (dynamical spin bath components are neglected): the driving field and the width of the dipolar field distribution b. In order to compare the model to a given Rabi oscillation experiment, we determine the driving field from the frequency of the Rabi oscillations at large pulse widths. The width b is determined independently from a Ramsey experiment. As shown in Fig. 3 of the main text, the main features of the experiment are reproduced in detail by the model. In Figs. S2 and S3 the dependence on the driving frequency is investigated. The experimentally observed shift of the collapse to longer pulse widths for higher driving frequencies is also seen in the analytical model. Small deviations between the model and the experiment, such as the slightly faster long-time decay in the experiment, may be explained by the dynamical components of the bath neglected in the model. The fact that the numerical simulations, which include the dynamical components, are closer to the experiment in this respect seems to confirm this.

At large magnetic field, when the NV center is described by a pseudo-spin $s_0 = 1/2$, the analysis can be performed in exactly the same way. In this case, for a given B_z,

$$p_0(t) = \cos^2 \Omega t/2 \tag{S32}$$

and, up to replacing $t \to t/2$, is the same as in the zero-magnetic field case, Eq. S27. Thus all results above remain the same, with the obvious modification $\tilde{b} \to b$. In particular, the contribution of $m_I = 0$ has the same form of slowly decaying ($1/\sqrt{t}$) oscillations with the time-varying phase. However, at large magnetic fields $A_0 \sim b$, and the contributions of $m_I = \pm 1$ do not differ crucially from the contributions of $m_I = 0$. Instead, the parts of the $P(B_z)$ distribution which are closer to zero have smaller value of v, and their decay is more of a power-law form, while the parts which are farther from zero have larger value of v, and their decay is faster, closer to the fast Gaussian decay. The corresponding experiment is shown in Fig. 4.

A few remarks are in order:

First, we note here that the Eqs. S29 and S31 can be obtained (with insignificant modifications) also in other cases, e.g. when $h_x \sim A_0$, $h_x \gg b$. The derivation above was chosen only

because it is physically more transparent, and allows to discuss the zero-magnetic field and the large-magnetic field cases on equal footings.

Second, it is worthwhile to note that exactly the same results can be obtained if, instead of the random field B_z, we had considered the full quantum bath (i.e., considered B_z as an operator) but assumming that the bath is static ($H_B = 0$). Consequently, in case of Rabi oscillations, again, the full quantum static bath is rigorously equivalent to static random field.

Finally, we briefly comment on the Rabi oscillations at 514 G, which demonstrate an interesting two-frequency pattern. At this magnetic field, the frequency of the Rabi driving field equals the transition frequency of both NV center, and the nitrogen atoms. However, the term describing the response of the NV center to the Rabi field (in the rotating frame) is of the form $(1/\sqrt{2})g_0\mu_B H_R s_0^x$, see Eq. S4. At the same time, the response of the nitrogen spins to the Rabi field is $\sqrt{2}$ times smaller. This corresponds to the experimental observations: the second Rabi frequency of the NV center is $\sqrt{2}$ times smaller than its "native" frequency, and corresponds to the Rabi frequency of the nitrogen atoms. The fact that the second frequency is present at very early times, of order of 0.1 μs, strongly suggests that already at zero time, an entanglement between the NV center and the nitrogen spins is present. The detailed description of this entangled state and its dynamics is currently under development.

6 Microscopic theory: Numerical simulations

The numerical simulations have been performed in the rotating frame, starting directly from the Hamiltonians given by Eqs. S3, S12, and S14 for zero magnetic field, and Eqs. S4, S13, and S14 for large magnetic field. The nuclear spins of the NV center and of the nitrogen P1 centers have been explicitly taken into account, as well as the dipolar interactions between the nitrogen spins.

The NV center was placed at the origin of the coordinate frame, and the nitrogen atoms have been randomly placed around the NV center. The distances to the nitrogen atoms have been all scaled by the same factor, to give the experimentally measured decay time of Ramsey fringes; this scaling factor is the only adjustable parameter in the numerical simulations. In this way, we obtained the correct local density of bath spins. Note that we did not average over positions of the nitrogens: such an averaging would correspond to the ensemble of the NV centers, and, as we discussed in Sec. 5.2, would not be correct for a measurement of a single NV center.

The state of the system was described by an exact many-spin wavefunction, including both the NV center and the nitrogen atoms. Initially, the state of the NV center was $|m_S = 0\rangle$, while the bath spins were in a random superposition of all possible bath basis states. This superposition state gives an excellent (exponentially accurate) approximation for the experimentally relevant state of the bath (maximally mixed, with the density matrix proportional to the identity matrix) (*S15*).

The dynamics of the system was simulated using an expansion of the time-evolution operator $\exp(-itH)$ in terms of Chebyshev polynomials (*S15*). The number of nitrogen atoms was

varied from $N = 4$ to $N = 6$. Simulations of larger systems is demanding, since the total number of basis states is large. For a single nitrogen atom, we need six basis states (two electron spin states, three nuclear spin states), so that the simulations with $N = 6$ involve 140,000 basis states ($\simeq 47,000$ basis states for the bath, multiplied by three basis states for the NV spin). At the same time, the simulation timestep should be kept small due to the large value of the Rabi driving field H_R, so that the total number of timesteps is large.

Moreover, we took into account the fact that each nitrogen can have different directions of the delocalization axis. The directions of the delocalization axes were randomly assigned for all nitrogens, and the averaging over 10 realizations was taken. Also, we performed averaging over three possible z-projections of the nuclear spin of the NV center; this projection is a constant of motion.

The simulations have been performed for all three types of relevant experiments: Ramsey fringes decay, Hahn spin echo decay, and damping of the Rabi oscillations. Fig. S4 shows simulations of the Hahn spin echo and the Ramsey experiment, for the same configuration of the P1 centers as in the simulation shown in Fig. 3. Fitting the simulations with our model equations yields values for both T_2 and b that agree with those of NV14 within error bars. Therefore, our analytical model and the numerical simulations seem to provide good description for decoherence of the NV centers, which is also reflected in the agreement between experiment and simulation in the Rabi oscillations.

References

S1. R. J. Epstein, F. M. Mendoza, Y. K. Kato and D. D. Awschalom, Nature Phys. **1**, 94 (2005).

S2. J. H. N. Loubser and J. A. van Wyk, Rep. Prog. Phys. **41**, 1201 (1978).

S3. P. W. Anderson and P. R. Weiss, Rev. Mod. Phys. **25**, 269 (1953); J. R. Klauder and P. W. Anderson, Phys. Rev. **125**, 912 (1962).

S4. R. Kubo, J. Phys. Soc. Japan **17**, 1100 (1962); R. Kubo, M. Toda, and N. Hashitsume, *Statistical Physics II* (Springer, Berlin, New York, 1998).

S5. R. de Sousa and S. Das Sarma, Phys. Rev. B **68**, 115322 (2003); W. M. Witzel and S. Das Sarma, Phys. Rev. B **74**, 035322 (2005).

S6. G. M. Zhidomirov and K. M. Salikhov, Sov. Phys. JETP **29**, 1037 (1969).

S7. J. Wrachtrup and F. Jelezko, J. Phys.: Cond. Mat. **18**, S807 (2006).

S8. X.-F. He, N. B. Manson, and P. T. H. Fisk, Phys. Rev. B **47**, 8816 (1993).

S9. R. J. Cook and D. H. Whiffen, Proc. R. Soc. London A **295**, 99 (1966).

S10. C. P. Slichter, *Principles of Magnetic Resonance* (Springer, Berlin, New York, 1990).

S11. A. Abragam, *Principles of Nuclear Magnetism* (Oxford University Press, Oxford, New York, 2004), Chapters IV.IV.A and IV.IV.B.

S12. V. V. Dobrovitski *et al.* (to be published).

S13. V. V. Dobrovitski et al., quant-ph/0112053; V. V. Dobrovitski et al., HAIT J. Sci. Eng. **1**, 586 (2005).

S14. F. H. L. Koppens et al., Phys. Rev. Lett. **99**, 106803 (2007).

S15. W. Zhang et al., J. Phys.: Cond. Matter **19**, 083202 (2007).

Supplementary Figure Captions

Figure S1. Spin echo measurements.

(**A**) Pulse sequence for the spin echo measurements. (**B**) Spin echo signal of NV31 at B = 0 G as a function of τ_2 for different τ_1. (**C**) Measurement of coherence time T_2 of NV31 using the spin echo pulse scheme of (A) with $\tau_1 = \tau_2 = \tau$. Fitting the data to $\exp(-2\tau/T_2)$ yields $T_2 = (0.62 \pm 0.09)$ μs at B = 0 G and $T_2 = (5.0 \pm 0.5)$ μs at B = 740 G.

Figure S2. Comparison of experiment with analytical model for Rabi oscillations of NV14 at *B* =0 G.

Experimental Rabi oscillations of NV14 (top panels) and calculations using our analytical model (bottom panels) with b = 0.42 MHz, for driving frequencies of (**A**) 11.7 MHz, (**B**) 21.4 MHz, and (**C**) 25.6 MHz.

Figure S3. Comparison of experiment with analytical model for Rabi oscillations of NV31 at *B* =0 G.

Experimental Rabi oscillations of NV31 (top panels) and calculations using our analytical model (bottom panels) with b = 0.47 MHz, for driving frequencies of (**A**) 12.1 MHz, (**B**) 15.3 MHz, and (**C**) 20.5 MHz.

Figure S4. Numerical simulation of spin echo and free evolution at *B* = 0 G.

Numerical simulations of the dynamics of a single NV spin surrounded by a bath of six nitrogen impurities at B = 0 G (see text). (**A**) Spin echo experiment. Fitting the numerical results yields $T_2 = (0.41 \pm 0.2)$ μs. (**B**) Free evolution. Fitting the numerical results with the value for T_2 found from (A) gives $b = (0.37 \pm 0.02)$ MHz.

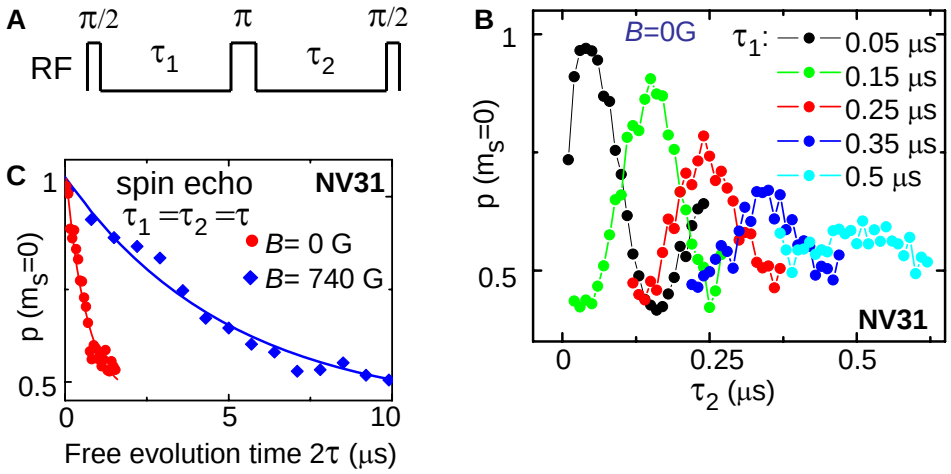

Figure S1. Hanson et al.

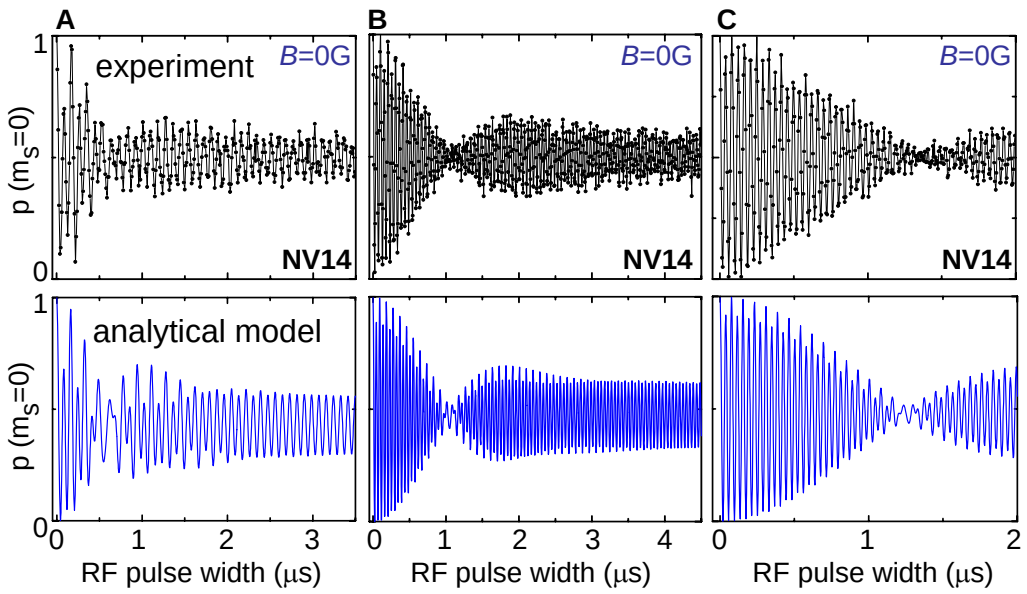

Figure S2. Hanson et al.

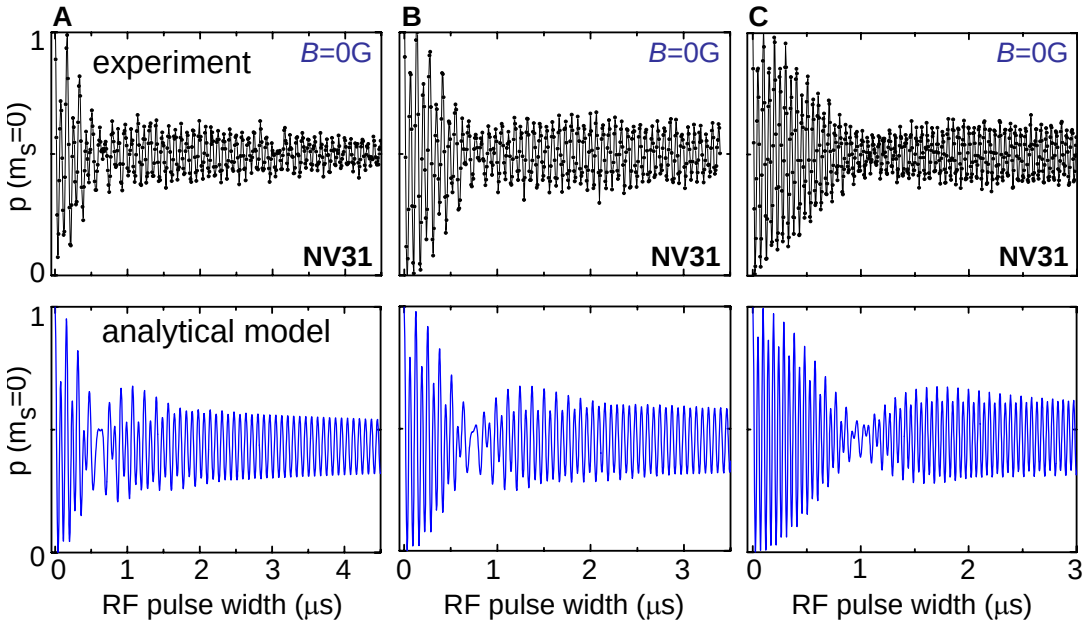

Figure S3. Hanson et al.

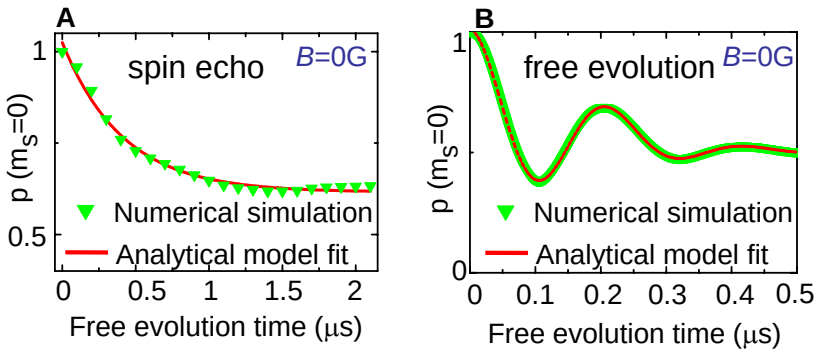

Figure S4. Hanson et al.